

PDE foundation model-accelerated inverse estimation of system parameters in inertial confinement fusion

Mahindra Rautela*, Alexander Scheinker*, Bradley Love †, Diane Oyen†, Nathan DeBardeleben‡, Earl Lawrence†, Ayan Biswas†

*AOT-IC Group, Los Alamos National Laboratory, Los Alamos, NM, USA

†CAI Division, Los Alamos National Laboratory, Los Alamos, NM, USA

‡HPC Division, Los Alamos National Laboratory, Los Alamos, NM, USA

Emails: {mrautela, ascheink, love, doyen, ndebard, earl, ayan}@lanl.gov

Abstract—PDE foundation models are typically pretrained on large, diverse corpora of PDE datasets and can be adapted to new settings with limited task-specific data. However, most downstream evaluations focus on forward problems, such as autoregressive rollout prediction. In this work, we study an inverse problem in inertial confinement fusion (ICF): estimating system parameters (inputs) from multi-modal, snapshot-style observations (outputs). Using the open *JAG benchmark*, which provides hyperspectral X-ray images and scalar observables per simulation, we finetune the PDE foundation model and train a lightweight task-specific head to jointly reconstruct hyperspectral images and regress system parameters. The fine-tuned model achieves accurate hyperspectral reconstruction (test MSE 1.2×10^{-3}) and strong parameter-estimation performance (up to $R^2 = 0.995$). Data-scaling experiments (5%–100% of the training set) show consistent improvements in both reconstruction and regression losses as the amount of training data increases, with the largest marginal gains in the low-data regime. Finally, finetuning from pretrained MORPH weights outperforms training the same architecture from scratch, demonstrating that foundation-model initialization improves sample efficiency for data-limited inverse problems in ICF.

Index Terms—Scientific Machine Learning, PDE Foundation Model, Plasma Physics, Inertial Confinement Fusion, Inverse problems

I. INTRODUCTION

Standalone PDE surrogate models have dominated scientific machine learning for a variety of physical applications. Some of the popular methods include physics-informed neural networks (PINNs) [1]; operator-learning methods such as DeepONet [2] and neural operators including Fourier neural operators (FNOs) [3], wavelet neural operators (WNOs) [4], Laplace neural operators [5], and physics-informed neural operators (PINOs) [6]; latent-state and reduced-order evolution models [7–11]; and continuous-depth dynamical models such as Koopman-based formulations with nonlinear forcing [12]

and neural ODEs (ODE-Nets) [13]. Despite their success, these models are typically developed and trained for a specific PDE, parameterized family, geometry, or discretization, and often require retraining (or substantial re-tuning) when the governing physics, resolution, or observational modality changes.

This motivates pretraining-based approaches that aim to amortize learning across PDE families and enable more data-efficient adaptation to new tasks and regimes. PDE foundation models are task-agnostic neural surrogates pretrained on large and diverse collections of PDE solution datasets to learn transferable representations, and then adapted via finetuning to specific downstream tasks [14]. Relative to training from scratch, this pretraining–finetuning paradigm can improve sample efficiency and generalization, especially when transferring to previously unseen PDE families, parameter regimes, or geometries [15, 16]. MORPH extends this idea to multi-modal scientific data by supporting heterogeneous PDE datasets across 1D–3D, varying spatial resolutions, and multiple physical fields with mixed scalar and vector components within a unified representation [17].

Inverse problems seek to infer latent causes such as material properties, boundary/initial conditions, or system/design parameters from indirect and often noisy observations generated by an underlying forward model [18]. In contrast to forward prediction, the inverse mapping is frequently ill-posed: the solution may be non-unique, unstable to perturbations in the data, or may not exist without incorporating additional prior information or regularization. Consequently, practical inversion typically relies on constraints, explicit regularizers, and/or sensitivity-informed diagnostics to obtain stable and physically plausible estimates [19].

While PDE foundation models have shown strong transfer and sample efficiency across forward modeling tasks, their use for inverse problems remains comparatively less explored. Most existing PDE foundation models are pretrained with autoregressive objectives on spatiotemporal datasets, and evaluation/finetuning commonly targets long-horizon rollouts [20]. Although inverse problems are not yet a primary focus

Research presented in this article was supported by the Laboratory Directed Research and Development program of Los Alamos National Laboratory under project number 20250637DI. This research used resources provided by the Los Alamos National Laboratory Institutional Computing Program, which is supported by the U.S. Department of Energy National Nuclear Security Administration under Contract No. 89233218CNA000001.

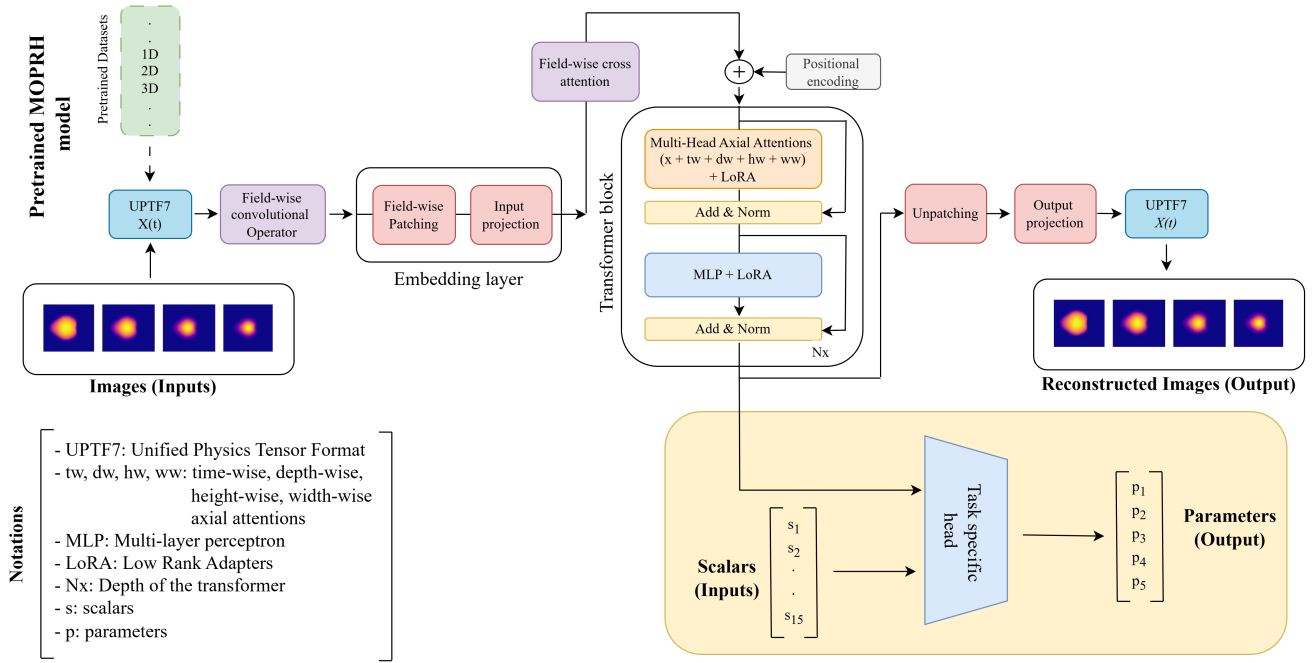


Fig. 1: Schematic illustrating how the PDE foundation model (MORPH) latent representation is coupled with a lightweight task-specific head. Hyperspectral images are provided as input to the foundation model, which is fine-tuned for reconstruction. The transformer-block outputs are passed to a task-specific head (a dense neural network). In parallel, the task-specific head (TSH) also ingests 15 scalar observables/diagnostics and is trained to predict a 5D parameter output. The foundation model and TSH are trained jointly end-to-end, using separate loss functions with independent optimizers and learning-rate schedulers.

in the PDE foundation-model literature, foundation models in other domains have been adapted to inverse tasks by attaching lightweight, task-specific heads (or decoders) on top of pretrained representations and finetuning only a small subset of parameters. This paradigm is well established in language [21] and vision [22]. More recently, it has become increasingly common in scientific foundation models, for example in chemistry and Earth-system modeling where pretrained backbones are repurposed for parameter inference, design, or reconstruction from partial observations [23, 24].

Recent works have explored a broad range of inverse problems in ICF. Humbird *et al.* [25] use Bayesian optimization to select drive inputs that maximize neutron yield with only a small number of experiments. Wang *et al.* [26] extend this idea with iterative multi-fidelity Bayesian optimization, using Gaussian-process surrogates to combine low- and high-fidelity evaluations while dynamically allocating simulation budget. For post-shot analysis, Gaffney *et al.* [27] employ an MCMC-based hierarchical Bayesian calibration framework to infer latent simulation inputs (and their shot-to-shot variability) that make radiation-hydrodynamics simulations consistent with sparse NIF diagnostic observations. On the diagnostic inversion side, Serino *et al.* [28] estimate physical/initial-condition parameters of a shock-driven instability experiment from noisy time-resolved radiographs using a feature-extraction-based, two-network learning pipeline. More recently, Gutierrez *et al.*

[29] study inverse design of laser pulse shapes by mapping desired implosion outcomes (and target parameters) to feasible drive profiles using diffusion and autoregressive generative models. In parallel, language-based foundation models are beginning to be applied to design-oriented ICF tasks, including spherical shell design and semi-empirical tuning to support experimental planning [30, 31].

In this work, we study an inverse problem estimating latent inertial confinement fusion (ICF) design parameters from multi-modal diagnostic observations and assess whether PDE foundation-model pretraining improves inversion accuracy and data efficiency relative to training from scratch. In the ICF setting considered here, the inverse task is to estimate the simulator input parameters from a multi-modal diagnostic signature consisting of hyperspectral images and scalar observables [32]. The key contributions of this work are:

- 1) *PDE foundation models for inverse problems.* We present (to our knowledge) one of the first demonstrations of adapting a PDE foundation model (MORPH) to an *inverse* task, moving beyond the forward-rollout settings that dominate prior PDE foundation-model evaluations.
- 2) *ICF parameter estimation from multi-modal diagnostics.* We formulate and evaluate an ICF inverse problem on the JAG benchmark by finetuning MORPH to estimate simulator/design parameters from multi-modal observations comprising hyperspectral X-ray images and scalar

diagnostics.

- 3) *Data-driven sensitivity analysis.* We introduce an interpretable sensitivity analysis (PCA compression of images + ridge regression over image PCs and scalars) to quantify parameter–observable dependence and identify weakly constrained (ill-posed) parameter directions.
- 4) *Systematic evaluation: scaling and scratch baselines.* We report data-scaling results (5%–100% training data) and a controlled training-from-scratch baseline using the *same* architecture, isolating the benefit of foundation-model initialization and showing the largest gains in the low-data regime.

II. METHODS

A. Dataset

We use the open ICF dataset released in the LLNL `mao` repository, generated with a 1D semi-analytic ICF simulator that models capsule implosion dynamics and produces a multi-modal suite of synthetic diagnostics [33]. This dataset is commonly referred to as the JAG benchmark and has been used in Refs. [32, 34–36]. Each simulation is specified by a five-dimensional input vector of design/physics parameters and yields two complementary observation modalities: (i) four spectrally resolved X-ray images (four energy bands) at 64×64 resolution and (ii) 15 scalar diagnostic quantities (e.g., yield, ion temperature, pressure, and related observables). We denote the parameter vector by $x \in \mathbb{R}^5$, the imaging observations by $y_{\text{img}} \in \mathbb{R}^{64 \times 64 \times 4}$, and the scalar diagnostics by $y_{\text{sc}} \in \mathbb{R}^{15}$. The dataset contains 10,000 samples generated by the simulator, which defines a forward mapping $f: x \mapsto y = (y_{\text{img}}, y_{\text{sc}})$.

B. Model

PDE foundation models are pretrained on large, heterogeneous corpora spanning multiple PDE benchmarks, and can be fine-tuned in data-limited regimes where they often outperform identical architectures trained from scratch [37]. However, scaling pretraining across diverse benchmarks introduces a central challenge: learning from multiple data modalities while handling variation in dimensionality, resolution, and field structure (including both scalar and vector-valued quantities) across PDE datasets. Naively padding all samples to a common shape is often infeasible at scale because simulation corpora can be extremely large (e.g., The Well is 15 TB) [38]. To address this, MORPH was designed to enable multi-modal training over larger and more diverse PDE corpora while keeping computation tractable [17].

Built on *Unified Physics Tensor Format* (UPTF-7), MORPH is a modality-agnostic architecture that addresses data heterogeneity through three complementary mechanisms (Fig. 1). First, *component-wise convolutions* operate over scalar and vector components to inject locality biases that improve sample efficiency. Second, *inter-field multi-head cross-attention* explicitly models coupling among distinct physical fields, enabling selective information transfer and robust feature fusion even when fields evolve on mismatched

spatial/temporal scales; it can also reduce cost by producing a single fused field representation. Finally, MORPH uses *4D axial attention* that factorizes spatiotemporal self-attention across time and spatial axes, reducing complexity from $O((TDHW)^2)$ to $O(T^2 + D^2 + H^2 + W^2)$ while retaining expressivity.

MORPH is pretrained with an autoregressive objective that predicts the next time step from previous states, enabling it to learn transferable spatiotemporal representations. Pretraining is performed on a heterogeneous corpus drawn from widely used PDE benchmarks [16, 38, 39], and the resulting model is then fine-tuned on multiple downstream forward-modeling tasks. The pretraining suite comprises six spatiotemporal datasets spanning 1D–3D domains with diverse field and component structure: 1D-CFD (computational fluid dynamics), 2D-DR (diffusion–reaction), 2D-SW (shallow water), 2D-CFD-IC (incompressible CFD/Navier–Stokes), 3D-MHD (magnetohydrodynamics), and 3D-CFD (computational fluid dynamics). In contrast, the physics governing ICF fusion and its hyperspectral X-ray signatures is not represented in this pretraining suite [40]. We therefore consider hyperspectral reconstruction and parameter inference for ICF as an out-of-distribution transfer setting. The codebase (including the model implementation and trained weights) for MORPH is open-sourced and publicly available in the associated repository**.

We leverage the pretrained MORPH backbone and attach a lightweight, task-specific head (TSH) to estimate system parameters from hyperspectral images and scalar diagnostics (Fig. 1). The hyperspectral image tensor is processed by MORPH under an image-reconstruction objective, producing reconstructed images at the output. Alongside the reconstructed output, we use the final latent representation at the end of the transformer blocks as the image embedding for parameter regression. The image embedding is passed through two `Conv1D`→`GELU`→`Dropout` blocks, followed by two `Linear`→`GELU`→`Dropout` blocks. In parallel, the 15-dimensional scalar diagnostics are encoded with a smaller MLP and concatenated with the resulting image features. The resulting fused representation is then fed to a final projection layer to predict the system parameters.

C. Sensitivity analysis

Before implementing the fine-tuning pipeline, we perform a sensitivity analysis to quantify how strongly the outputs depend on the input parameters [41]. This is a useful preprocessing step for inverse problems because it provides an empirical indicator of ill-posedness: weak or non-unique dependence of the observables on certain parameters suggests poor identifiability and an inherently under-constrained inversion. By highlighting which observables carry information about which inputs, sensitivity analysis helps diagnose ill-posed parameter directions and guides model design and target selection, even without detailed expert knowledge of the simulator [19].

We study a data-driven linear sensitivity analysis for an inverse problem with multi-modal observations. Each sample

**<https://github.com/lanl/MORPH>

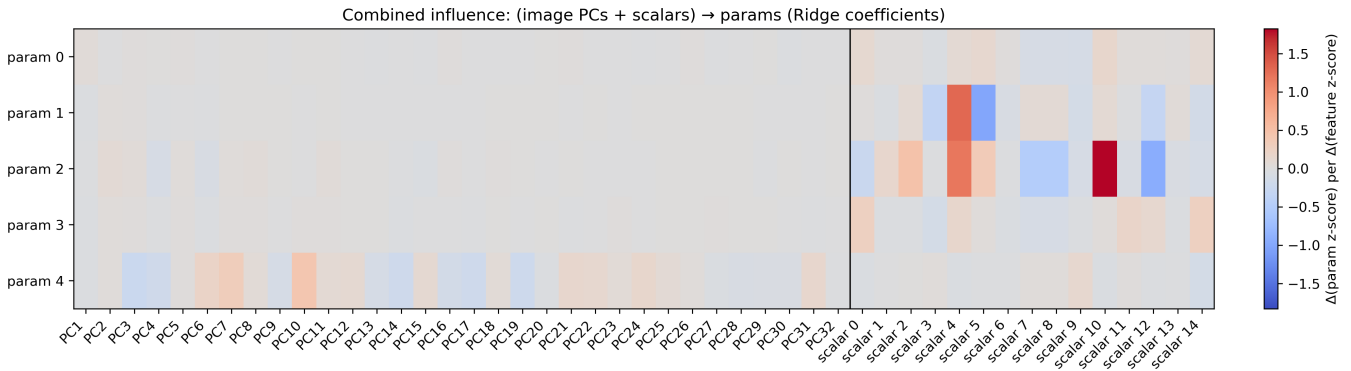


Fig. 2: Ridge-regression sensitivity map for predicting the five parameters from multi-modal features. Columns show standardized image PCA scores (PC1–PC32) and scalar diagnostics (scalar0–scalar14), separated by the vertical line; colors denote signed coefficient magnitude. The strongest dependencies are scalar-driven for `param1` and `param2`, while `param0` and `param3` exhibit near-zero coefficients, indicating poor identifiability.

comprises an image-like tensor $I \in \mathbb{R}^{64 \times 64 \times 4}$ together with a vector of scalar descriptors $s \in \mathbb{R}^{15}$, and the objective is to infer a low-dimensional parameter vector $y \in \mathbb{R}^5$. Because the image modality is high-dimensional, we vectorize I into $x \in \mathbb{R}^{64 \cdot 64 \cdot 4}$ and apply feature-wise standardization. This normalization removes scale effects, improves numerical conditioning, and makes regression coefficients comparable across heterogeneous modalities.

To obtain a compact and interpretable representation of the image channel, we apply principal component analysis (PCA) to the standardized image vectors and retain the leading K components, yielding latent image coordinates $z \in \mathbb{R}^K$. We then employ ridge regression to construct stable linear relationships between variables of interest. Ridge regularization (equivalently, Tikhonov regularization) mitigates ill-conditioning and multicollinearity, which commonly arise in high-dimensional inverse problems, and provides a well-posed surrogate for local, linearized sensitivity in the reduced space [42].

To quantify the joint contribution of both modalities to parameter inference, we concatenate the reduced image features and scalar descriptors into a single feature vector $h = [z; s] \in \mathbb{R}^{K+15}$ and fit a ridge model mapping h to standardized parameters. The resulting coefficient matrix enables transparent attribution: weights associated with PCA coordinates summarize image-driven dependence, whereas weights associated with the scalar entries capture the influence of auxiliary measurements.

III. RESULTS

A. Sensitivity results

Fig. 2 summarizes the learned ridge coefficients for the combined model (image principal components + scalars) → parameters. Overall, parameters exhibit markedly different levels of sensitivity to the available observables. Parameters `param1` and `param2` show clear, structured dependence on a subset of scalar descriptors, with several coefficients attaining

substantially larger magnitude than the background level. In contrast, the image PCA coordinates contribute weakly for these parameters, suggesting that the scalar channel carries most of the predictive signal in this linearized sensitivity analysis.

The image modality contributes more visibly to `param4`, which displays non-negligible weights across multiple PCA components (albeit with smaller magnitude than the strongest scalar effects observed for `param2`). This pattern indicates that `param4` is at least partially encoded in spatial/field structure captured by the dominant PCA modes, whereas the scalar descriptors play a comparatively minor role.

Most importantly, `param0` and `param3` exhibit near-zero coefficients across both feature blocks, indicating weak dependence on the measured observables under this linear surrogate. Consistent with this observation, these parameters achieve very low held-out R^2 compared to the remaining parameters, implying poor predictability and limited identifiability from the current observation set. In practice, this suggests that accurately recovering `param0` and `param3` will be difficult without additional information (e.g., more informative scalar diagnostics, richer image features, alternative measurement modalities, or stronger priors, larger training set), and motivates treating their inversion as intrinsically more ill-posed than the other parameters.

In prior studies [32, 36], substantially larger training sets are available (on the order of 10^5 samples), whereas the public repository used here provides only $\sim 10^4$ samples. Access to more data can improve the effective posedness of the inverse problem by better constraining the parameter–observation map, expanding coverage of the parameter space (and thus the diversity of observable responses), and reducing estimator variance. Motivated by our sensitivity analysis, we therefore focus on a reduced inversion task and predict only three of the five parameters, excluding the two parameters that exhibit consistently weak signal and poor prediction performance.

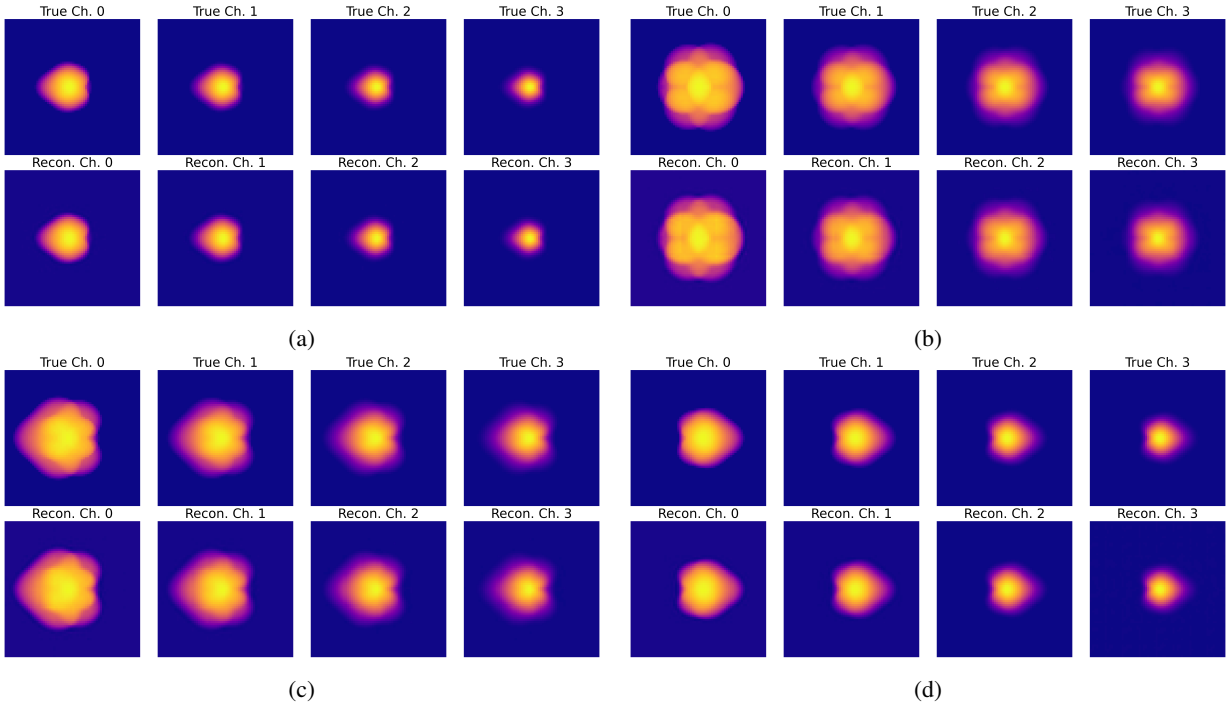


Fig. 3: Reconstruction results on four held-out test samples (a-d). For each example, the top row shows the ground-truth four-channel hyperspectral image, and the bottom row shows the corresponding reconstructed (predicted) image. Across the full test set, the recorded MSE between true and reconstructed images is 0.0012.

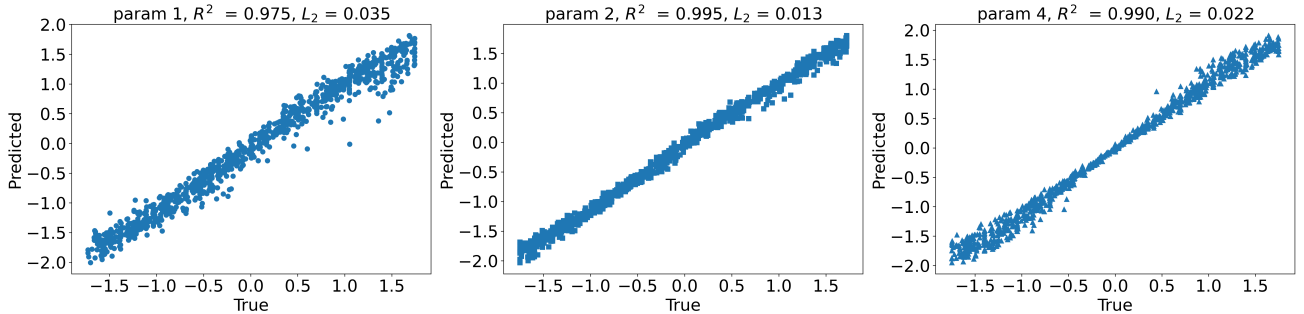


Fig. 4: Parameter estimation results on the test set. Scatter plots compare ground-truth versus predicted values for each of the three predicted parameters. We achieve strong agreement for three parameters: Param1 attains $R^2 = 0.975$ with $L_2 = 0.035$, Param2 attains $R^2 = 0.995$ with $L_2 = 0.013$, and Param4 attains $R^2 = 0.990$ with $L_2 = 0.022$.

B. Finetuning results

Among the four open-source MORPH foundation-model variants: MORPH-Ti (~ 7 M parameters), MORPH-S (~ 30 M), MORPH-M (~ 126 M), and MORPH-L (~ 480 M), we have selected MORPH-S for this study. We fine-tune all parameters of MORPH-S and train the task-specific head (TSH), which has ~ 1 M parameters, for a total of 100 epochs on a single RTX-A6000 GPU. The 10K-sample dataset is randomly split into train/val/test with an 80%/10%/10% ratio.

For both MORPH and TSH, we use the AdamW optimizer with weight decay 0.01, with learning rates of 10^{-4} for MORPH and 10^{-5} for TSH. We apply the same learning-rate schedule to both components: linear warmup for 5 epochs

(minimum LR 10^{-7}) followed by cosine decay. We use a batch size of 8 and optimize mean-squared error (MSE) losses for both the reconstruction and parameter-regression objectives.

1) *Hyperspectral image reconstruction*: Fig. 3 shows qualitative reconstruction results on four held-out test samples (a-d). For each example, the top row presents the ground-truth four-channel hyperspectral image and the bottom row shows the corresponding reconstruction. MORPH accurately reconstructs hyperspectral test images, including complex multi-lobe structures (e.g., Fig. 3b). Across the full test set, the reconstruction MSE is 1.2×10^{-3} , indicating that the pretrained backbone learns representations that preserve the essential spectral and spatial structure of the images.

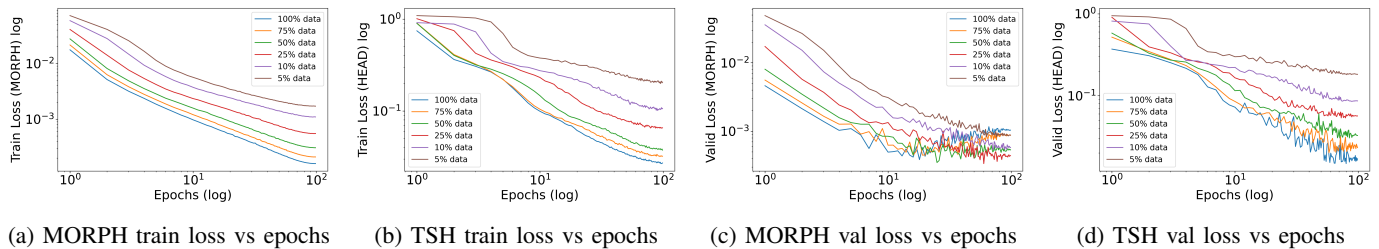


Fig. 5: Data-scaling study showing training and validation loss curves (log-log scale) as the fraction of available training data is varied (5%, 10%, 25%, 50%, 75%, and 100%). (a) MORPH reconstruction training loss, (b) task-specific head (TSH) parameter-regression training loss, (c) MORPH reconstruction validation loss, and (d) TSH parameter-regression validation loss, all plotted versus epochs (log-scaled axes).

2) *Parameter estimation*: Fig. 4 reports parameter estimation performance on the test set via scatter plots of predicted versus ground-truth values. Due to ill-posedness and limited sensitivity for some inputs, we evaluate three parameters (Param1, Param2, and Param4). The predictions are tightly concentrated around the diagonal, with Param2 exhibiting near-linear agreement across the full range. Quantitatively, Param1 achieves $R^2 = 0.975$ with $L_2 = 0.035$, Param2 achieves $R^2 = 0.995$ with $L_2 = 0.013$, and Param4 achieves $R^2 = 0.990$ with $L_2 = 0.022$. The overall regression MSE on the test set is 0.0235, demonstrating that the fine-tuned MORPH representations support accurate inverse estimation for the identifiable subset of parameters.

3) *Scaling studies*: We perform data-scaling experiments by varying the fraction of available training data while keeping the same optimization and training hyperparameters. Figure 5 summarizes the training and validation dynamics for six data regimes (5%, 10%, 25%, 50%, 75%, and 100% of the training set), reported on log-log axes. Across both objectives i.e., hyperspectral image reconstruction (MORPH) and parameter regression (TSH) increasing the training set size consistently reduces loss. For MORPH, the reconstruction training loss decreases monotonically with data fraction (Fig. 5a), indicating more effective fitting with additional supervision. On the validation set (Fig. 5c), the largest gains occur when scaling from 5% to 25%, after which the curves begin to cluster, suggesting diminishing returns for reconstruction beyond moderate data availability. We also observe mild late-epoch degradation in validation loss for some fractions. In practice, early stopping would mitigate this effect, while the overall scaling trend remains clear. In contrast, the task-specific head exhibits sustained improvements with more data: both the regression training loss (Fig. 5b) and validation loss (Fig. 5d) continue to decrease up to 75–100% of the data.

Overall, these results confirm that additional data yields more stable training dynamics and improvement in loss for both reconstruction and parameter estimation. These trends suggest further gains are likely as larger ICF datasets become available.

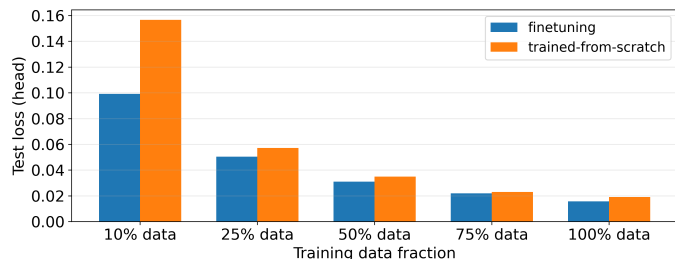


Fig. 6: fine-tuned model vs trained-from-scratch: Test-set parameter-regression loss of the TSH versus training-data fraction, comparing MORPH finetuning from pretrained weights to training the same architecture from scratch. Finetuning achieves lower loss, with the largest gains in the low-data regime (e.g., 10%), and the gap narrows as more training data becomes available.

C. Comparisons

We compare MORPH fine-tuning with a matched training-from-scratch baseline that uses the identical architecture and hyperparameters, with the only difference being whether weights are initialized from pretrained checkpoints. This controlled comparison isolates the effect of pretraining and quantifies its benefit in a data- and compute-limited regime. Fig. 6 compares the test-set parameter-regression loss of the task-specific head (TSH) when (i) finetuning MORPH from pretrained weights versus (ii) training the identical architecture from scratch, across multiple training-data fractions. Finetuning yields lower test loss in the most data-limited regime, with a pronounced improvement at 10% of the data, highlighting the sample-efficiency benefit of pretraining. As the training fraction increases (25%–100%), the gap progressively narrows, although finetuning remains consistently better, suggesting that pretraining provides the greatest advantage when supervision is scarce and its relative benefit diminishes as more labeled data becomes available.

Overall, these results show that adding training data improves both reconstruction and parameter estimation, while also stabilizing the learning dynamics. This scaling behavior suggests that further gains are likely as larger ICF datasets

become available.

CONCLUSIONS

We investigated PDE foundation-model transfer for an inverse ICF parameter-estimation task using the JAG benchmark, where multi-modal diagnostics (hyperspectral images and scalar observables) are used to infer simulator input parameters. A sensitivity analysis indicated that two parameters are weakly identifiable under the available observables, making the full inversion ill-posed and motivating a reduced task focused on three parameters. Finetuning MORPH-S with a lightweight task-specific head achieves accurate hyperspectral reconstruction (test MSE 1.2×10^{-3}) and strong parameter-estimation performance (up to $R^2 = 0.995$ on the best-predicted parameter). Data-scaling and baseline comparisons show that pretraining improves sample efficiency, yielding lower test loss than training from scratch, with the largest gains in the low-data regime. These results suggest PDE foundation models are a promising building block for data-limited inverse problems in ICF, and motivate future work on improving sensitivity via a larger training set, richer diagnostics, stronger priors, and more robust inverse objectives.

REFERENCES

- [1] M. Raissi, P. Perdikaris, and G. Karniadakis, “Physics-informed neural networks: A deep learning framework for solving forward and inverse problems involving nonlinear partial differential equations,” *Journal of Computational Physics*, vol. 378, pp. 686–707, 2019.
- [2] S. Goswami, K. Kontolati, M. D. Shields, and G. E. Karniadakis, “Deep transfer operator learning for partial differential equations under conditional shift,” *Nature Machine Intelligence*, vol. 4, no. 12, pp. 1155–1164, 2022.
- [3] Z. Li, N. Kovachki, K. Azizzadenesheli, B. Liu, K. Bhattacharya, A. Stuart, and A. Anandkumar, “Fourier neural operator for parametric partial differential equations,” *arXiv preprint arXiv:2010.08895*, 2020.
- [4] T. Tripura and S. Chakraborty, “Wavelet neural operator for solving parametric partial differential equations in computational mechanics problems,” *Computer Methods in Applied Mechanics and Engineering*, vol. 404, p. 115783, 2023.
- [5] Q. Cao, S. Goswami, and G. E. Karniadakis, “Laplace neural operator for solving differential equations,” *Nature Machine Intelligence*, vol. 6, no. 6, pp. 631–640, 2024.
- [6] Z. Li, H. Zheng, N. Kovachki, D. Jin, H. Chen, B. Liu, K. Azizzadenesheli, and A. Anandkumar, “Physics-informed neural operator for learning partial differential equations,” *ACM/JMS Journal of Data Science*, vol. 1, no. 3, pp. 1–27, 2024.
- [7] V. Oommen, K. Shukla, S. Goswami, R. Dingreville, and G. E. Karniadakis, “Learning two-phase microstructure evolution using neural operators and autoencoder architectures,” *npj Computational Materials*, vol. 8, no. 1, p. 190, 2022.
- [8] R. Maulik, B. Lusch, and P. Balaprakash, “Reduced-order modeling of advection-dominated systems with recurrent neural networks and convolutional autoencoders,” *Physics of Fluids*, vol. 33, no. 3, 2021.
- [9] M. Rautela, A. Williams, and A. Scheinker, “A conditional latent autoregressive recurrent model for generation and forecasting of beam dynamics in particle accelerators,” *Scientific Reports*, vol. 14, no. 1, p. 18157, 2024.
- [10] K. Kontolati, S. Goswami, G. Em Karniadakis, and M. D. Shields, “Learning nonlinear operators in latent spaces for real-time predictions of complex dynamics in physical systems,” *Nature Communications*, vol. 15, no. 1, p. 5101, 2024.
- [11] M. Rautela, A. Williams, and A. Scheinker, “Time-inversion of spatiotemporal beam dynamics using uncertainty-aware latent evolution reversal,” *Physical Review E*, vol. 111, no. 2, p. 025307, 2025.
- [12] M. Khodkar and P. Hassanzadeh, “A data-driven, physics-informed framework for forecasting the spatiotemporal evolution of chaotic dynamics with nonlinearities modeled as exogenous forcings,” *Journal of Computational Physics*, vol. 440, p. 110412, 2021.
- [13] R. T. Chen, Y. Rubanova, J. Bettencourt, and D. K. Duvenaud, “Neural ordinary differential equations,” *Advances in neural information processing systems*, vol. 31, 2018.
- [14] S. Subramanian, P. Harrington, K. Keutzer, W. Bhimji, D. Morozov, M. W. Mahoney, and A. Gholami, “Towards foundation models for scientific machine learning: Characterizing scaling and transfer behavior,” *Advances in Neural Information Processing Systems*, vol. 36, pp. 71 242–71 262, 2023.
- [15] Z. Hao, C. Su, S. Liu, J. Berner, C. Ying, H. Su, A. Anandkumar, J. Song, and J. Zhu, “Dpot: Autoregressive denoising operator transformer for large-scale pde pre-training,” *arXiv preprint arXiv:2403.03542*, 2024.
- [16] M. Herde, B. Raonic, T. Rohner, R. Käppeli, R. Molinaro, E. de Bézenac, and S. Mishra, “Poseidon: Efficient foundation models for pdes,” *Advances in Neural Information Processing Systems*, vol. 37, pp. 72 525–72 624, 2024.
- [17] M. S. Rautela, A. Most, S. Mansingh, B. C. Love, A. Biswas, D. Oyen, and E. Lawrence, “Morph: Pde foundation models with arbitrary data modality,” *arXiv preprint arXiv:2509.21670*, 2025.
- [18] C. R. Vogel, *Computational methods for inverse problems*. SIAM, 2002.
- [19] M. Rautela, A. Huber, J. Senthilnath, and S. Gopalakrishnan, “Inverse characterization of composites using guided waves and convolutional neural networks with dual-branch feature fusion,” *Mechanics of Advanced Materials and Structures*, vol. 29, no. 27, pp. 6595–6611, 2022.
- [20] S. Mansingh, J. Amarel, R. Arnab, A. Mohan, K. Singh, G. J. Kunde, N. Hengartner, B. Migliori, E. Casleton, N. A. Debardeleben *et al.*, “Towards reason-

- ing for pde foundation models: A reward-model-driven inference-time-scaling algorithm,” *arXiv preprint arXiv:2509.02846*, 2025.
- [21] T. Brown, B. Mann, N. Ryder, M. Subbiah, J. D. Kaplan, P. Dhariwal, A. Neelakantan, P. Shyam, G. Sastry, A. Askell *et al.*, “Language models are few-shot learners,” *Advances in neural information processing systems*, vol. 33, pp. 1877–1901, 2020.
- [22] M. Oquab, T. Darcet, T. Moutakanni, H. Vo, M. Szafraniec, V. Khalidov, P. Fernandez, D. Haziza, F. Massa, A. El-Nouby *et al.*, “Dinov2: Learning robust visual features without supervision,” *arXiv preprint arXiv:2304.07193*, 2023.
- [23] A. Wadell, A. Bhutani, V. Azumah, A. R. Ellis-Mohr, C. Kelly, H. Zhao, A. K. Nayak, K. Hegazy, A. Brace, H. Lin *et al.*, “Foundation models for discovery and exploration in chemical space,” *arXiv preprint arXiv:2510.18900*, 2025.
- [24] C. Bodnar, W. P. Bruinsma, A. Lucic, M. Stanley, A. Allen, J. Brandstetter, P. Garvan, M. Riechert, J. A. Weyn, H. Dong *et al.*, “A foundation model for the earth system,” *Nature*, pp. 1–8, 2025.
- [25] K. D. Humbird and J. L. Peterson, “Transfer learning driven design optimization for inertial confinement fusion,” *Physics of Plasmas*, vol. 29, no. 10, 2022.
- [26] J. Wang, N. Chiang, A. Gillette, and J. L. Peterson, “A multifidelity bayesian optimization method for inertial confinement fusion design,” *Physics of Plasmas*, vol. 31, no. 3, 2024.
- [27] J. A. Gaffney, K. Humbird, A. Kritcher, M. Kruse, E. Kur, B. Kustowski, R. Nora, and B. Spears, “Data-driven prediction of scaling and ignition of inertial confinement fusion experiments,” *Physics of Plasmas*, vol. 31, no. 9, 2024.
- [28] D. A. Serino, E. Bell, M. Klasky, B. S. Southworth, B. Nadiga, T. Wilcox, and O. Korobkin, “Physics consistent machine learning framework for inverse modeling with applications to icf capsule implosions,” *Scientific Reports*, vol. 15, no. 1, p. 25915, 2025.
- [29] R. L. Gutierrez, V. Gundecha, R. Ejaz, V. Gopalaswamy, R. Betti, S. Ghorbanpour, A. Lees, and S. Sarkar, “Implpg: Inverse modeling approach to laser pulse shape generation in inertial confinement fusion,” in *NeurIPS 2025 AI for Science Workshop*, 2025.
- [30] R. Bahukutumbi, D. D. Meyerhofer, N. Debardeleben, M. Lang, A. Jhunjhunwala, A. Vem, D. Luu, P. Gurumurthy, S. Halverson, G. Gupta *et al.*, “Fine-tuning large language models for inertial confinement fusion—a collaboration with nvidia,” in *DPP 2025*. APS, 2025.
- [31] M. Grosskopf, R. Bent, R. Somasundaram, I. Michaud, A. Lui, N. Debardeleben, and E. Lawrence, “Ursa: The universal research and scientific agent,” *arXiv preprint arXiv:2506.22653*, 2025.
- [32] R. Anirudh, J. J. Thiagarajan, P.-T. Bremer, and B. K. Spears, “Improved surrogates in inertial confinement fusion with manifold and cycle consistencies,” *Proceedings of the National Academy of Sciences*, vol. 117, no. 18, pp. 9741–9746, 2020.
- [33] J. A. Gaffney, R. Anirudh, P.-T. Bremer, J. Hammer, D. Hysom, S. A. Jacobs, J. L. Peterson, P. Robinson, B. K. Spears, P. T. Springer, J. J. Thiagarajan, B. Van Essen, and J.-S. Yeom, “The jag inertial confinement fusion simulation dataset for multi-modal scientific deep learning.” In Lawrence Livermore National Laboratory (LLNL) Open Data Initiative. UC San Diego Library Digital Collections., 3 2020. [Online]. Available: <https://library.ucsd.edu/dc/object/bb5534097t>
- [34] R. Anirudh, J. J. Thiagarajan, S. Liu, P.-T. Bremer, and B. K. Spears, “Exploring generative physics models with scientific priors in inertial confinement fusion,” *arXiv preprint arXiv:1910.01666*, 2019.
- [35] S. A. Jacobs, B. Van Essen, D. Hysom, J.-S. Yeom, T. Moon, R. Anirudh, J. J. Thiagarajan, S. Liu, P.-T. Bremer, J. Gaffney *et al.*, “Parallelizing training of deep generative models on massive scientific datasets,” in *2019 IEEE International Conference on Cluster Computing (CLUSTER)*. IEEE, 2019, pp. 1–10.
- [36] A. Shukla, Y. Mubarka, R. Anirudh, E. Kur, D. Mariscal, B. Djordjevic, B. Kustowski, K. Swanson, B. Spears, P.-T. Bremer *et al.*, “On the design and evaluation of generative models in high energy density physics,” *Communications Physics*, vol. 8, no. 1, p. 14, 2025.
- [37] A. Marcato, A. Pachalieva, R. G. Hill, K. Gao, X. Wang, E. Rougier, Z. Lei, V. Agrawal, J. Chua, Q. Kang *et al.*, “A foundation model for material fracture prediction,” *arXiv preprint arXiv:2507.23077*, 2025.
- [38] R. Ohana, M. McCabe, L. Meyer, R. Morel, F. Agocs, M. Beneitez, M. Berger, B. Burkhart, S. Dalziel, D. Fielding *et al.*, “The well: a large-scale collection of diverse physics simulations for machine learning,” *Advances in Neural Information Processing Systems*, vol. 37, pp. 44 989–45 037, 2024.
- [39] M. Takamoto, T. Praditia, R. Leiteritz, D. MacKinlay, F. Alesiani, D. Pflüger, and M. Niepert, “Pdebench: An extensive benchmark for scientific machine learning,” *Advances in Neural Information Processing Systems*, vol. 35, pp. 1596–1611, 2022.
- [40] J. Gaffney, P. Springer, and G. Collins, “Thermodynamic modeling of uncertainties in nif icf implosions due to underlying microphysics models,” in *APS Division of Plasma Physics Meeting Abstracts*, vol. 2014, 2014, pp. PO5–011.
- [41] K. Balasubramaniam, “Inversion of the ply lay-up sequence for multi-layered fiber reinforced composite plates using genetic algorithm,” *Nondestructive Testing and Evaluation*, vol. 15, no. 5, pp. 311–331, 1998.
- [42] A. Björkström, “Ridge regression and inverse problems,” *Stockholm University, Department of Mathematics*, 2001.